

Experimental coherent-state quantum secret sharing with finite pulses

Yuan-Zhuo Wang,^{1,2,*} Xiao-Ran Sun,^{1,2,*} Xiao-Yu Cao,^{1,2,*} Hua-Lei Yin,^{2,1,3,†} and Zeng-Bing Chen^{1,‡}

¹*National Laboratory of Solid State Microstructures and School of Physics,*

Collaborative Innovation Center of Advanced Microstructures, Nanjing University, Nanjing 210093, China

²*Department of Physics and Beijing Key Laboratory of Opto-electronic Functional Materials and Micro-nano Devices,*

Key Laboratory of Quantum State Construction and Manipulation (Ministry of Education),

Renmin University of China, Beijing 100872, China

³*Beijing Academy of Quantum Information Sciences, Beijing 100193, China*

(Dated: October 10, 2024)

Quantum secret sharing (QSS) plays a significant role in multiparty quantum communication and is a crucial component of future quantum multiparty computing networks. Therefore, it is highly valuable to develop a QSS protocol that offers both information-theoretic security and validation in real optical systems under a finite-key regime. In this work, we propose a three-user QSS protocol based on phase-encoding technology. By adopting symmetric procedures for the two players, our protocol resolves the security loopholes introduced by asymmetric basis choice without prior knowledge of the identity of the malicious player. Kato's concentration inequality is exploited to provide security against coherent attacks with the finite-key effect. Moreover, the practicality of our protocol has been validated under a 30-dB channel loss with a transmission distance of 5-km fiber. Our protocol achieves secure key rates ranging from 432 to 192 bps by choosing different pulse intensities and basis selection probabilities. Offering enhanced security and practicality, our protocol stands as an essential element for the realization of quantum multiparty computing networks.

I. INTRODUCTION

Multiparty quantum communication, a key element in realizing quantum multiparty computing networks, offers information-theoretic security that surpasses the limitations of classical cryptography. [1–19]. As a cryptographic component of quantum communication technologies, quantum secret sharing (QSS) has garnered significant interest for its potential in multiparty quantum communication networks [20–29]. In the scenario of secret sharing, each party possesses a portion of the information, with the complete key reconstructed only through collaboration among authorized parties. This is the fundamental concept of the secret sharing scheme, initially introduced independently by Shamir [30] and Blakley [31]. The security of the classical secret sharing scheme relies on computational complexity, which has been proven to be vulnerable under the rapid development of quantum computing technology [32, 33].

QSS was proposed to address this issue. In 1999, Hillery, Buzek, and Berthiaume utilized the entanglement properties of the Greenberger-Horne-Zeilinger (GHZ) state to construct a QSS protocol [24]. This protocol divides a message from a dealer into two parts and distributes them to two players, in such a way that both parts of the split message are necessary to reconstruct the original message. Numerous QSS protocols were proposed in succession [25, 26, 34–42] while the feasibility of QSS protocols was verified through experiments [27–29, 43–46]. Despite the advancements, existing QSS pro-

ocols still face challenges in terms of security, efficiency, and practicality. For instance, the original three-user GHZ-based QSS protocol is vulnerable if one player is dishonest [38]. Over the past few decades, protocols employing sequential single-qubit transmission have been proposed to circumvent the need for GHZ states [45, 47, 48]. However, these single-qubit protocols have drawbacks in terms of security, failing to resist Trojan horse attacks [49–51]. In recent years, differential phase-shift QSS schemes have been developed employing weak coherent states to simplify the experimental setup [52–54]. However, this kind of QSS protocol exhibits security limitations, offering resistance only against individual attacks. The round-robin QSS schemes have gained popularity in recent years due to their inherent advantages, including high noise tolerance and resistance against signal disturbances [55, 56]. However, the practical implementation of this scheme is constrained by the requirement of a variable-delay Mach-Zehnder interferometer at the dealer's end. Recently, a QSS protocol encoding logic bits in weak coherent states, which does not require intensity modulation and phase randomization, has been proposed [57]. However, the protocol exhibits asymmetry in certain steps for different participants, necessitating prior knowledge of the eavesdropper's identity and potentially introducing security loopholes.

In this paper, we propose a tripartite QSS protocol. Our protocol utilizes phase encoding with weak coherent states, a method validated in numerous phase-encoded quantum key distribution (QKD) protocols [13, 58, 59]. Our protocol adopts a similar single-photon interference approach as twin-field QKD [8, 60, 61], which allows the key rate to scale with the square root of the total transmittance between the two players. These features simplify implementation by eliminating the need for phase

* These authors contributed equally.

† hlyin@ruc.edu.cn

‡ zbchen@nju.edu.cn

randomization and intensity modulation. By adopting symmetric procedures for all players during key generation and error-rate analysis, our protocol achieves secure key generation without requiring prior knowledge of the dishonest player's identity, thus addressing security loopholes arising from asymmetric basis choices in previous protocols [57]. We adopt Kato's inequality, which offers tighter bounds compared to the commonly used Azuma's inequality, to provide security against coherent attacks for finite-key analysis [62, 63]. We further optimize the final secure key rates using Kato's inequality [64, 65], achieving transmission distances over 200 km with a misalignment error rate of 1.5% and exceeding 150 km even with a higher misalignment error rate of 4.5%. Furthermore, we experimentally demonstrate our QSS protocol under a 30-dB channel loss, including a 5-km fiber distance. We implement nine sets of tests with varying pulse intensities and X -basis selection probabilities, analyzing their impacts on secure key rates. We successfully achieve the best key rate of 432 bps with the intensity of 9×10^{-4} and the probability of 0.9. While this work focuses on a tripartite QSS protocol, the demand for multiuser quantum communication is growing [66, 67]. Expanding QSS to accommodate more users is a crucial challenge for future development. Promisingly, our protocol shares similarities with twin-field QKD, which can be extended to multiuser scenarios via time-division multiplexing with a Sagnac network setup [68]. Exploring similar strategies to increase the user capacity of our protocol will be a key direction for future research. With its enhanced security, practicality, and high key rates, our protocol contributes to the groundwork for future large-scale quantum multi-party computing networks.

II. PROTOCOL DESCRIPTION

We show the schematic of our protocol in Fig. 1. Two symmetric distant participants, Alice and Bob, act as the players of our QSS protocol. They each encode their logic bits and basis selections onto the phase of weak coherent pulses, send them to the central dealer Charlie. Alice and Bob use phase modulators (PMs) to encode the information and variable optical attenuators (VOAs) to dim the pulses. Charlie receives the pulses and, after applying a phase modulation to Bob's pulse, allows them to interfere at the beam splitter. Eventually, Charlie records the detection events of the two superconducting nanowire single-photon detectors, SPD₁ and SPD₂. The detailed steps of our scheme are as follows:

1. **Preparation.** In the i th round, Alice and Bob each choose a bit value uniformly at random and record them as $s_{a,i}$ and $s_{b,i}$, where a and b denote Alice and Bob, respectively. Then, they each select a basis choice a_i and b_i from $\{X, Y\}$ with probabilities p_x for the X basis and $1 - p_x$ for the Y basis. Based on the chosen values, they each prepare a weak coherent pulse to represent their quantum bit and send it to Charlie. If the X basis is cho-

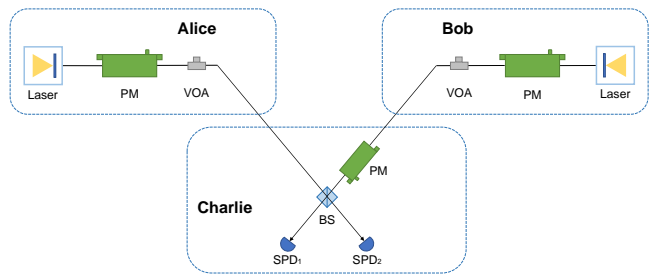


FIG. 1. Schematic of our QSS scheme. Alice and Bob send weak coherent pulses to Charlie for interference measurement, with Charlie announcing the corresponding detection results. Alice and Bob encode their pulses with phase modulators (PMs) and use variable optical attenuators (VOAs) to attenuate their pulses to the single-photon level. After adding a phase of $\{0, \pi/2\}$ on Bob's pulses based on his basis selection, Charlie performs interference measurement with a beam splitter (BS) and two superconducting nanowire single-photon detectors, SPD₁ and SPD₂.

sen, Alice prepares the pulse $|e^{i s_{a,i} \pi} \sqrt{\mu}\rangle_A$, and Bob prepares the pulse $|e^{i s_{b,i} \pi} \sqrt{\mu}\rangle_B$, where the subscript A and B denote the channel mode of Alice and Bob. If the Y basis is chosen, Alice prepares the pulse $|e^{i(-s_{a,i} + \frac{\pi}{2})\pi} \sqrt{\mu}\rangle_A$, and Bob prepares the pulse $|e^{i(-s_{b,i} + \frac{\pi}{2})\pi} \sqrt{\mu}\rangle_B$.

2. **Measurement.** Charlie selects a basis choice c_i from $\{X, Y\}$ with probabilities p_x for the X basis and $1 - p_x$ for the Y basis. Then, he modulates Bob's pulse with an extra phase of $\pi/2$ if the chosen basis is Y , and leaves Bob's pulse unmodulated if the chosen basis is X . After the two pulses from Alice and Bob interfere at a beam splitter (BS), Charlie performs the measurement using two detectors, SPD₁ and SPD₂. There are four possible outcomes $\{0, 1, \emptyset, \perp\}$ where 0 is the case when SPD₁ clicks and 1 is the case when SPD₂ clicks. Cases with no detection are denoted as \emptyset . Double detection events are denoted as \perp , in which case Charlie randomly chooses a logic bit from $\{0, 1\}$. According to the outcomes, Charlie assigns his bit value $s_{c,i}$.

3. **Basis reconciliation.** After announcing their basis choices over an authenticated public channel, all participants identify the following sets: $\mathcal{X} := \{i : a_i = b_i = c_i = X \wedge s_{c,i} \neq \emptyset\}$, $\mathcal{Y}_{bc} := \{i : b_i = c_i = Y \wedge a_i = X \wedge s_{c,i} \neq \emptyset\}$, and $\mathcal{Y}_{ac} := \{i : a_i = c_i = Y \wedge b_i = X \wedge s_{c,i} \neq \emptyset\}$, where the subscripts a , b , and c denote Alice, Bob, and Charlie, respectively. They then verify that the sizes of these sets meet the required thresholds for key generation: $|\mathcal{X}| \geq n_X$, $|\mathcal{Y}_{bc}| \geq n_{Y_{bc}}$, and $|\mathcal{Y}_{ac}| \geq n_{Y_{ac}}$, where n_X , $n_{Y_{bc}}$, and $n_{Y_{ac}}$ are predetermined thresholds correlated with the desired key length. Steps 1-3 are repeated until these conditions are met, and the number of rounds required to fulfill these conditions is denoted as N .

4. **Raw key generation and error estimation.** Based on the basis reconciliation results, the participants sift their bits. The bit pairs satisfying $S_X := \{\{s_{a,i}, s_{b,i}, s_{c,i}\} : i \in \mathcal{X}\}$ are used to generate the secure key bits, with a portion of these bits dedicated to

analyzing the bit error rate E_b^X . For the bit pairs satisfying $\{s_{a,i}, s_{b,i}, s_{c,i}\} : i \in \mathcal{Y}_{ac}$, Charlie's corresponding bit is flipped: $s'_{c,i} = s_{c,i} \oplus 1$. This forms a set of key bits $S_{Y_{ac}} := \{\{s_{a,i}, s_{b,i}, s'_{c,i}\} : i \in \mathcal{Y}_{ac}\}$. These bits, along with those satisfying $S_{Y_{bc}} := \{\{s_{a,i}, s_{b,i}, s_{c,i}\} : i \in \mathcal{Y}_{bc}\}$, are revealed and used independently to calculate the phase error rates E_{pac} and E_{pbc} . The higher of these two error rates is then used to calculate the upper bound of the final phase error rate \bar{E}_p . Finally, the error rates are checked against predetermined thresholds, E_b^{tol} for the bit error rate and E_p^{tol} for the phase error rate. If either $E_b^X > E_b^{\text{tol}}$ or $\bar{E}_p > E_p^{\text{tol}}$, indicating potential information leakage exceeding security requirements, the protocol aborts. Otherwise, the protocol proceeds to the next step.

5. Postprocessing. All participants perform error correction, where the amount of information leakage, λ_{EC} , is revealed. Then, to ensure that they share data with the perfect correlation, they perform an error-verification step using a random universal₂ hash function that publishes $\log_2 2/\epsilon_c$ bits of information. Following successful error correction, privacy amplification is performed to distill the final secure keys: S_a , S_b , and S_c by applying a random universal₂ hash function. The final keys satisfy the following conditions: $S_c = S_a \oplus S_b$ and $|S_a| = |S_b| = |S_c| = \ell$ bits, in which ℓ represents the length of the final generated key.

III. SECURITY ANALYSIS

This section provides a comprehensive security analysis of our proposed protocol. We assume a perfect source is utilized in our protocol to simplify the analysis. We analyze the protocol step-by-step to ensure the generated secure key meets the requirements of a secret sharing scheme. We then demonstrate our protocol's resistance against malicious players attempting to steal information from other participants. We focus solely on internal eavesdroppers, as the potential information leakage to them exceeds that of external eavesdroppers, ensuring this approach does not compromise the protocol's overall security. We establish an equivalence between the security of our protocol against internal eavesdroppers and that of phase-encoded QKD. This allows us to leverage the well-established security of phase-encoded QKD to effectively verify the security of our QSS protocol [58, 59]. Subsequently, we show that the security analysis of the protocol is symmetrical concerning the two different players, avoiding the security loopholes introduced by asymmetric protocol steps. Finally, we obtain the secure key rate of our protocol by analyzing the information leakage that a malicious player can obtain from other participants.

A. Secure key bit correlation

In the i th round, Alice and Bob each randomly choose a bit value, recorded as $s_{a,i}$ and $s_{b,i}$, respectively. Charlie then sets his bit value, $s_{c,i}$, based on the measurement outcome. QSS protocols require a specific correlation between the key bits. This involves dividing a secret from the dealer into two parts and distributing them to two players in such a way that both parts of the split secret are necessary to reconstruct the original secret. This is achieved by setting Charlie's raw key bits to the exclusive OR (XOR) of Alice and Bob's raw key bits, denoted as $S_c = S_a \oplus S_b$. We will show that the keys generated by our protocol satisfy this correlation.

As shown in the first step of our protocol, Alice (Bob) prepares weak coherent states denoted as $|e^{is_{a,i}\pi\sqrt{\mu}}\rangle_A$ ($|e^{is_{b,i}\pi\sqrt{\mu}}\rangle_B$) under the X basis, and $|e^{i(-s_{a,i}+\frac{3}{2})\pi\sqrt{\mu}}\rangle_A$ ($|e^{i(-s_{b,i}+\frac{3}{2})\pi\sqrt{\mu}}\rangle_B$) under the Y basis, with μ denoting the pulse intensity. Due to the 2π periodicity, the weak coherent states under the Y basis can also be expressed as $|e^{i(s_{a,i}-\frac{1}{2})\pi\sqrt{\mu}}\rangle_A$ ($|e^{i(s_{b,i}-\frac{1}{2})\pi\sqrt{\mu}}\rangle_B$). In the second step, Charlie modulates an extra 0 ($\pi/2$) phase to Bob's pulse under X (Y) basis.

The two optical modes sent by Alice and Bob can be described using the annihilation operators a_A and a_B , respectively: $|\alpha\rangle_A = e^{-|\alpha|^2/2}e^{\alpha a_A^\dagger}|0\rangle_A$ and $|\alpha\rangle_B = e^{-|\alpha|^2/2}e^{\alpha a_B^\dagger}|0\rangle_B$, where $\alpha = \sqrt{\mu}e^{i\theta}$ represents the complex amplitude of the coherent state and $|0\rangle$ represents the vacuum state, with μ being the laser intensity and $e^{i\theta}$ the laser phase. The two modes are combined in the beam splitter after their phases are modulated by the phase modulators. Based on the quantum description of the beam splitter, the outgoing annihilation operators a_1 and a_2 , corresponding to the two single-photon detectors SPD₁ and SPD₂, respectively, are expressed as $a_1 = (a_B + a_A)/\sqrt{2}$ and $a_2 = (a_B - a_A)/\sqrt{2}$. Since the two pulses have the same intensity μ , the response of SPD₁ or SPD₂ is determined solely by the phase difference between the two pulses incident on the beam splitter. If the phase difference is 0 , only SPD₁ will click. If the phase difference is π , only SPD₂ will click. If the phase difference is $\pi/2$ or $3\pi/2$, both detectors have an equal probability of clicking. For the key bits in S_X and $S_{Y_{bc}}$ generated during the i th round, the phase difference is given by $\Delta\Phi = (s_{b,i} - s_{a,i})\pi$. Charlie sets his logic bit to 0 (1) upon SPD₁ (SPD₂) clicks, resulting in $s_{c,i} = s_{a,i} \oplus s_{b,i}$. For the key bits in $S_{Y_{ac}}$ generated during the i th round, the phase difference is given by $\Delta\Phi = (s_{b,i} - s_{a,i} + 1)\pi$. With Charlie's bit flipped: $s'_{c,i} = s_{c,i} \oplus 1$, the key bit correlation remains $s'_{c,i} = s_{a,i} \oplus s_{b,i}$. Thus, the final keys S_a , S_b , and S_c satisfy the correlation: $S_c = S_a \oplus S_b$.

It is worthwhile to note that our discussion thus far assumes ideal scenarios. Under these ideal conditions, the generated secure key fulfills the requirements of a secret sharing scheme.

B. Security equivalence

We provide a detailed description of the security equivalence between our QSS protocol and the phase-encoded QKD protocol. To establish the security equivalence, we first introduce the phase-encoded QKD protocol, as shown in Fig. 2 (a). The phase-encoded QKD protocol involves two participants, Alice and Bob. Alice chooses a basis out of X and Y . Based on the chosen basis, Alice emits a signal pulse and encodes her logic bit on the phase of the signal pulse. In X basis, Alice emits a weak coherent pulse $|e^{i s_{a,i} \pi} \sqrt{\mu}\rangle_A$, where $s_{a,i}$ is the logic bit of Alice in the i th round and μ is the intensity of the pulse. In Y basis, Alice emits a weak coherent pulse $|e^{i(-s_{a,i} + \frac{\pi}{2})\pi} \sqrt{\mu}\rangle_A$. Alice also emits a reference pulse $|\sqrt{\mu}\rangle_A$ as an ancillary pulse and sends both pre-

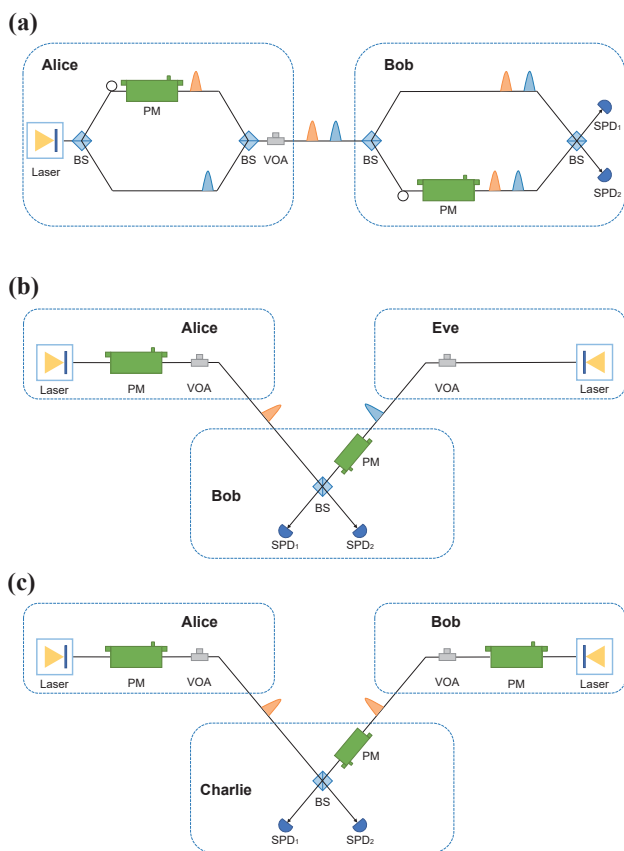


FIG. 2. Schematic diagrams of the phase-encoded QKD protocol, its variant, and our QSS protocol. (a) Schematic of the original phase-encoded QKD protocol. Each round, Alice prepares a signal pulse (orange) using her phase modulator and a reference pulse (blue) before sending them to Bob. Bob modulates the phases of the pulses and then performs a two-pulse interference. The phase difference is obtained to generate a secure key bit. (b) An equivalent variant of the phase-encoded protocol, where an eavesdropper Eve sends the reference pulse instead of Alice. (c) Schematic of our QSS protocol, where Bob replaces the eavesdropper and modulates his pulse using a phase modulator.

pared pulses to Bob. Bob chooses a basis out of X and Y and applies a phase modulation of 0 (π) on the signal pulse when the chosen basis is X (Y). Bob then allows the two pulses to interfere and measures the phase difference, obtaining his logic bit based on the measurement results. Alice and Bob retain their logic bits as raw key bits when they choose the same basis and discard them otherwise. In the X basis, they use the raw key bits to generate the final key and estimate the bit error rate. In the Y basis, they use the raw key bits to bound the phase error rate.

We then consider a variant of our scheme and demonstrate the equivalence between its security against an internal eavesdropper and the security of the phase-encoded QKD protocol. As an intermediate step, we consider a variant of the phase-encoded QKD protocol, as shown in Fig. 2 (b). In this variant, Alice transmits only the signal pulses, while an eavesdropper, Eve, sends the reference pulses. These pulses arrive simultaneously at Bob's location and interfere. In the phase-encoded QKD protocol, even if an eavesdropper knows the relative phase of the reference pulse, they cannot obtain information about the secret key [58]. This ensures the security of the variant protocol.

Finally, regardless of whether Alice or Bob acts as the eavesdropper, our QSS protocol is equivalent to the variant of the phase-encoded QKD protocol. As shown in Fig. 2 (c), this variant retains the preparation and measurement steps of the original scheme but modifies the sifting and parameter estimation steps. Since the potential phase information added by an eavesdropper does not compromise the security of phase-encoded QKD, and our protocol demonstrates equivalent security against internal eavesdroppers, we have established the security of our QSS protocol against an internal malicious player.

C. Eavesdropper's identity

We establish the security of our protocol by demonstrating its equivalence to the phase-encoded QKD protocol, thus leveraging existing security proofs [58, 59]. However, existing security proofs for the phase-encoded QKD protocol assume honest participants with complete trust, while eavesdroppers are completely distrusted. In our protocol, the malicious player's identity is revealed only during the use of raw key bits to bound error rates and when the two players collaborate to obtain information from Charlie. Before this stage, we have no information about the malicious player's identity. Therefore, the basis choice in the sifting process must be symmetric for both Alice and Bob during the generation of secure key bits. This symmetry is crucial to ensure protocol security even if Alice and Bob's roles were interchanged. As demonstrated in our protocol the key bits in S_X are used to form their secure key and use a portion of it to estimate the bit error rate. This process is symmetric for both Alice and Bob. Ideally, they would disclose

the logic bits under the corresponding chosen bases to bound the phase error rate based on the internal eavesdropper's identity. Specifically, if Alice were the internal eavesdropper, the logic bits in $S_{Y_{bc}}$ would be revealed to bound the phase error rate; if Bob were the internal eavesdropper, the logic bits in $S_{Y_{ac}}$ would be revealed instead. However, since the internal eavesdropper's identity remains unknown, both steps must be executed in the protocol's practical implementation. The higher of the two resulting values, representing the worst-case information leakage scenario, is selected as the phase error rate.

D. Information leakage

We now analyze the security of the variant scheme in the scenario where Bob acts as the internal eavesdropper. Since Bob acts as the eavesdropper, his secure key information is naturally fully known to the eavesdropper. Therefore, our security analysis of the variant focuses on the potential leakage of Alice's pulse phase information. This analysis is conducted by introducing a "quantum coin" into our system and considering an equivalent protocol.

Imagine a coin that Alice flips for each signal she sends. The coin has two sides, representing her two choices of encoding basis for the key bit. If the coin is perfectly fair (50/50 probability for each side), Eve gains no information about Alice's basis choice just by observing the coin flips. This corresponds to the ideal scenario where the signals themselves reveal nothing about the chosen basis.

However, in a practical scenario with weak coherent states, the signals are not perfectly basis independent. This is analogous to Alice having a slightly biased coin. The bias, though small, could allow Eve to gain partial information about the chosen basis, potentially compromising the protocol's security.

The "quantum coin" in our analysis precisely captures this basis dependence. It is not a physical coin, but a mathematical tool to quantify how much information Eve could extract about Alice's basis choice based on the inherent properties of the emitted signals.

We first denote Alice's basis-dependent states as

$$|\Psi_x\rangle = (|0_X\rangle \otimes |\alpha\rangle + |1_X\rangle \otimes |-\alpha\rangle)/\sqrt{2} \quad (1)$$

$$|\Psi_y\rangle = (|1_Y\rangle \otimes |i\alpha\rangle + |0_Y\rangle \otimes |-i\alpha\rangle)/\sqrt{2} \quad (2)$$

where $|0_X\rangle, |1_X\rangle$ are eigenstates of the Pauli operator σ_x and $|0_Y\rangle, |1_Y\rangle$ are eigenstates of the Pauli operator σ_y . Then, Alice measures the state of the quantum coin under $|0_Z\rangle, |1_Z\rangle$ basis and chooses her states $|\Psi_x\rangle$ or $|\Psi_y\rangle$ according to the result. Note that we assume the measurement is delayed till the eavesdropper finishes eavesdropping on the signals. We can denote the joint state of the quantum coin state and Alice's source state as

$$|\Phi\rangle = \sqrt{p_x}|0_Z\rangle \otimes |\Psi_x\rangle + \sqrt{p_y}|1_Z\rangle \otimes |\Psi_y\rangle, \quad (3)$$

where p_x and p_y denote the probabilities of Alice selecting the X basis and Y basis, respectively, to encode her signals. Introducing the quantum coin establishes a relationship between the basis dependence of Alice's signal and the imbalance Δ of the quantum coin. This allows us to quantify the basis dependence and bound the information leakage of Alice's pulses.

The logic bits in $S_{Y_{ac}}$ and $S_{Y_{bc}}$ are used to calculate the phase errors. The basis dependence of Alice's signals, denoted by Δ , is calculated as

$$1 - 2Q_\mu\Delta = \langle \Psi_y | \Psi_x \rangle, \quad (4)$$

where Q_μ denotes the protocol's total gain. The phase error rate E_p is then calculated using the formula

$$E_p = E_b^Y + 4\Delta(1 - \Delta)(1 - 2E_b^Y) + 4(1 - 2\Delta)\sqrt{\Delta(1 - \Delta)E_b^Y(1 - E_b^Y)}, \quad (5)$$

where E_b^Y is the bit error rate calculated using the key bits in $S_{Y_{ac}}$ or $S_{Y_{bc}}$.

The final key rate of our protocol is expressed as

$$R = Q_\mu[1 - f_e H(E_b^X) - H(E_p)], \quad (7)$$

where f_e is the error-correction efficiency, E_b^X is the bit error rate of the raw key bits in S_X , and $H(x) = -x \log_2 x - (1 - x) \log_2 (1 - x)$ is the Shannon entropy. The total gain Q_μ for the key bits in S_X is calculated as $Q_\mu = (1 - p_d)[1 - (1 - 2p_d)e^{-2\mu\eta}]$, where p_d is the dark count rate of both of Charlie's detectors and μ is the light intensity of the weak coherent states. The bit error rate E_b^X is given by $E_b^X Q_\mu = e_d(1 - p_d)[1 - (1 - p_d)e^{-2\mu\eta}] + (1 - e_d)p_d(1 - p_d)e^{-2\mu\eta}$, where e_d is the misalignment error rate of the detectors.

IV. SIMULATIONS

This section evaluates the performance of our protocol in the finite-key regime and practical implementations through theoretical simulations. We first clarify the specific security criteria employed in our analysis. For small errors in our protocols $\epsilon_c, \epsilon_s > 0$, our protocol is $\epsilon_c + \epsilon_s$ secure if it is ϵ_c correct and ϵ_s secret. The ϵ_c -correctness condition is satisfied if $\Pr[S_c \neq S_a \oplus S_b] \leq \epsilon_c$, i.e., the secret key bits satisfy the correlation except with a small probability ϵ_c . The ϵ_s -secrecy condition is satisfied if $(1 - p_{\text{abort}})|\rho_{CE} - U_C \otimes \rho_E|_{1/2} \leq \epsilon_s$ where ρ_{CE} is the classical-quantum state describing the joint state of S_c and the system of the eavesdropper E , U_C is the uniform mixture of all possible values of S_c , and p_{abort} is the probability that the protocol aborts. The symbol ϵ_{PA} denotes the failure probabilities of privacy amplification. In practice, we have $\epsilon_s = \sqrt{\epsilon} + \epsilon_{PA}$, where ϵ is the failure probability of the phase error rate estimation.

In the finite-key regime, conditioned on passing the error-estimation and error-verification steps, the secure

key rate of our protocol is given by

$$\ell = n_X [1 - H(\overline{E}_p)] - \lambda_{\text{EC}} - \log_2 \frac{2}{\epsilon_c} - \log_2 \frac{1}{4\epsilon_{PA}^2}, \quad (8)$$

where n_X denotes the size of the set \mathcal{X} . The term $\lambda_{\text{EC}} = n_X f_e H(E_b^X)$ denotes the number of bits consumed during the error-correction process. Here, f_e denotes the error-correction efficiency, and E_b^X denotes the bit error rate of the key bits in S_X . A detailed analysis of the upper bound for the observed phase error rate \overline{E}_p is provided in Appendix A.

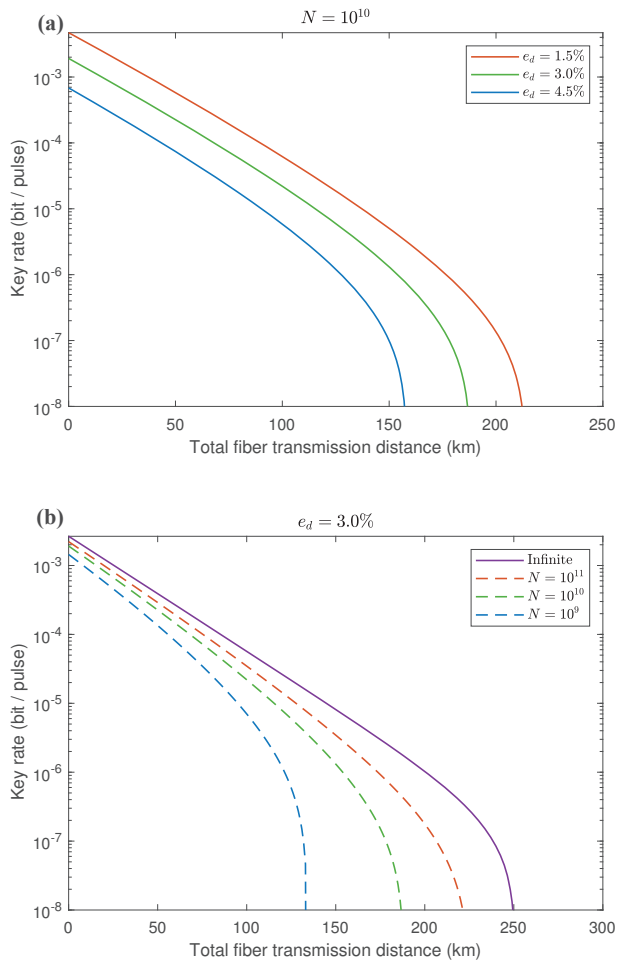


FIG. 3. Secure key rates of our protocol under the finite-key regime for different misalignment error rates e_d and total numbers of pulses N . (a) The total number of pulses N is fixed at 10^{10} , a typical value in practical deployments. The misalignment error rates e_d are set to 1.5%, 3.0%, and 4.5%. The key rates demonstrate that our protocol can generate secure keys over distances exceeding 200 km with a relatively low misalignment error rate of 1.5% in practical implementations. (b) The misalignment error rate e_d is fixed at 3.0%, while the values of the total number of pulses are $N = 10^9$, 10^{10} , 10^{11} , and an infinite regime. As N increases, the secure key rates of our protocol approach the performance of the ideal infinite-key scenario, with distances exceeding 200 km achieved when $N = 10^{11}$.

We consider the distance between Alice and Bob as L , resulting in their distances to the central participant Charlie being $L/2$ each. This leads to a total channel transmittance η of $\eta_d \times 10^{-\alpha L/20}$, where η_d is the detection efficiency of Charlie's detectors and α is the attenuation coefficient of the ultra-low-loss fiber used in our simulations. This demonstrates that the secure key rate of our protocol scales with the square root of the total distance between Alice and Bob, similar to the twin-field quantum key distribution setup [8]. Our simulations use parameters conforming to the actual experimental apparatus: $\eta_d = 40\%$, $p_d = 2 \times 10^{-8}$, $\alpha = 0.167$, and $f_e = 1.16$. Under these conditions, we incorporate pulse intensities and X -basis selection probabilities as parameters into the optimization algorithm to obtain optimal secure key rates for different distance scenarios. As shown in Fig. 3 (a), we fix the total number of pulses to $N = 10^{10}$, a typical value in real experimental deployments. By setting different misalignment error rates e_d to 1.5%, 3.0%, and 4.5%, we obtain the secure key rates of our protocol under different misalignment error rates. The simulation result from Fig. 3 (a) shows that our protocol can achieve a transmission distance exceeding 150 km under the condition of the misalignment error rates $e_d = 4.5\%$. This suggests the practicality of our protocol in field tests and real-world implementations, where misalignment errors are likely to occur. Figure. 3 (b) presents the simulation results for a fixed misalignment error rate $e_d = 3.0\%$ and varying total numbers of pulses $N = 10^9$, 10^{10} , 10^{11} , and infinite. As shown, the secure key rates of our protocol increase with the total number of pulses, achieving transmission distances exceeding 200 km when $N = 10^{11}$. A detailed finite-key analysis is provided in Appendix A.

V. EXPERIMENTAL DEMONSTRATION

Our QSS experimental setup is depicted in Fig. 4. On Charlie's side, a continuous-wave laser source (NKT Koheras BASIK E15) with a center wavelength of 1550.12 nm and a linewidth less than 0.1 kHz is used. Two intensity modulators (IMs) are used to chop the continuous wave into a pulse train, achieving a pulse extinction ratio of over 30 dB. The resulting pulses have a temporal width of less than 1 ns and a repetition rate of 100 MHz. Subsequently, the pulses pass through a circulator (Cir) and are then split into two identical pulses by a 50:50 BS.

The two pulses enter the Sagnac loop, which guarantees phase stability between Alice and Bob. Within the loop, the pulses are modulated by Alice, Bob, and Charlie. Notably, Alice (Bob) uses a PM to encode the counterclockwise (clockwise) pulses exclusively. The basis selection is performed with probabilities p_x and p_y for the X and Y bases. A random phase of 0 or π is added for the X basis, while a phase of $\pi/2$ or $3\pi/2$ is added for the Y basis. Specifically, Charlie randomly adds a phase of 0 or $\pi/2$ to Bob's pulses with probabilities p_x and p_y , re-

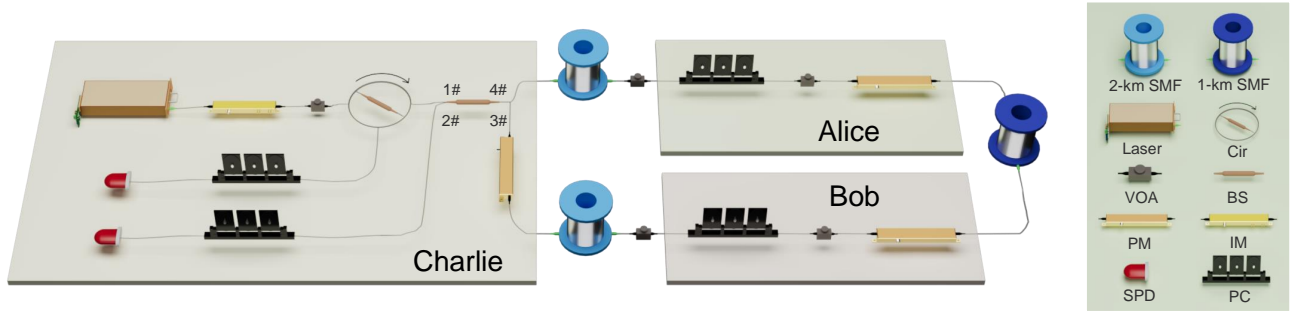


FIG. 4. Schematic of our QSS experimental setup. Continuous wave is chopped by two intensity modulators (IMs) into a pulse train, which is split into two identical pulses by a 50:50 BS. The two pulses enter the Sagnac loop and are modulated by Alice, Bob, and Charlie, respectively. After traveling through the loop, the two modulated pulses interfere at Charlie's BS and are detected by two SPDs. SMF, single-mode fiber; Cir, circulator; PC, polarization controller.

spectively. The system includes 2-km single-mode fibers (SMFs) connecting Alice and Bob to Charlie, and a 1-km SMF connecting Alice and Bob. Additionally, polarization controllers (PCs) are placed between the PMs and SMFs to ensure polarization alignment.

The two modulated pulses interfere at Charlie's BS. Charlie uses two SPDs to detect the interference results. The detection efficiencies of SPDs are 39.3% and 39.5%, with dark count rates of 2.8×10^{-8} and 4.0×10^{-8} within 2-ns time windows. To compensate for the differing detection efficiencies, which affect the ratio of 0 and 1 in the raw keys, Charlie employs a PM to add an extra phase of 0 or π to Bob's pulses with equal probability (50% each). The total channel attenuation between Alice and Bob is 30 dB. To simulate a symmetric channel, an additional attenuation of approximately 2.5 dB is added between

Alice and Charlie to balance Charlie's PM loss.

We implemented our protocol and investigated the impact of the pulse intensity μ and the selection probability of X basis p_x on secure key rates. Theoretical simulation predicts the highest key rate at $\mu = 9 \times 10^{-4}$ when p_x is 0.9. To optimize performance, we, respectively, chose the intensities of 9×10^{-4} , 8×10^{-4} , and 7×10^{-4} and the probabilities of 0.9, 0.8, and 0.7 to perform nine sets of tests. The accumulation time is 500 seconds and the data size for each test is 5×10^{10} . Detailed experimental data under different input values of μ and p_x are provided in Appendix B. After collecting all data, we calculated the experimental quantum bit error rates (QBERs), phase error rates, and secure key rates. Table I lists the experimental data.

As shown in Fig. 5, the highest key rate 432 bps is achieved with $p_x = 0.9$ and $\mu = 9 \times 10^{-4}$. With the decrease of p_x and μ , the final key rate tends to be lower. Since the detection events under X basis are used to generate final key bits, the key rates is directly related to p_x . The results confirm that reducing the X -basis selection probability leads to a decrease in the final key rate under the same pulse intensity. With higher intensity, the number of detections increases, but more information is leaked, leading to an increased phase error rate. Additionally, other experimental parameters, such as QBERs in the X basis and Y basis, also influence the results. For a fixed X -basis selection probability, both pulse intensity and error rate affect the key rate. Therefore, as the intensity decreases, the key rate under the same probability of X basis does not always decrease. The largest QBER observed in our experiment is less than 1.8%, which shows our protocol can resist environmental interference and has robustness.

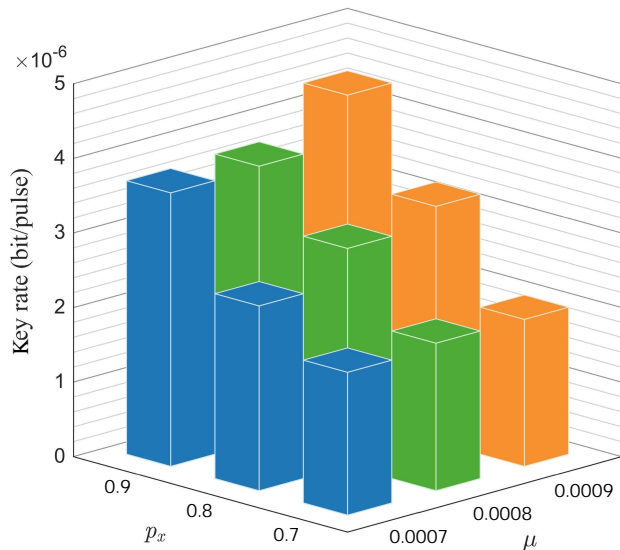


FIG. 5. Key rates of our QSS scheme vs pulse intensities, μ , and X -basis selection probabilities, p_x . Varying the intensities 7×10^{-4} , 8×10^{-4} and 9×10^{-4} and X -basis selection probabilities 0.9, 0.8, and 0.7, yields secure key rates ranging from 432 to 192 bps.

VI. CONCLUSION

In summary, we have proposed a QSS protocol utilizing phase encoding on weak coherent states to eliminate the need for phase randomization and intensity modulation.

TABLE I. Summary of experimental results. The total data size is 5×10^{10} . p_x denotes the X -basis selection probability, μ is the higher intensity of the pulses sent by Alice and Bob, E_b^X and E_b^Y are the experimental quantum bit error rates in the X and Y bases, respectively, E_p is the phase error rate, n_x and n_y are the numbers of detections in the X and Y bases, respectively, and SKR is the secure key rate.

p_x	μ	E_b^X (%)	E_b^Y (%)	E_p (%)	n_x	n_y	SKR(bit/pulse)
0.9	9×10^{-4}	0.95	1.16	15.66	787 407	18 056	4.32×10^{-6}
	8×10^{-4}	1.03	1.37	15.55	683 629	15 889	3.70×10^{-6}
	7×10^{-4}	1.05	1.30	14.18	606 878	13 769	3.67×10^{-6}
0.8	9×10^{-4}	1.05	1.27	14.99	561 372	72 686	3.16×10^{-6}
	8×10^{-4}	0.99	1.44	14.57	494 329	63 721	2.92×10^{-6}
	7×10^{-4}	1.12	1.79	14.46	430 832	55 912	2.48×10^{-6}
0.7	9×10^{-4}	1.07	1.57	15.66	377 194	133 361	1.97×10^{-6}
	8×10^{-4}	0.99	1.44	14.32	330 782	117 229	1.98×10^{-6}
	7×10^{-4}	0.92	1.53	13.37	292 026	104 446	1.92×10^{-6}

The same single-photon interference method as the twin-field QKD is used in our protocol, allowing the key rate to scale with the square root of the channel transmittance. By employing a symmetric basis choice for all participants during secure key generation and error-rate analysis, our protocol achieves secure key generation without prior knowledge of the dishonest player's identity, addressing the security loopholes associated with asymmetric basis choices compared to the previous protocols. Additionally, we employed Kato's inequality instead of the more commonly used Azuma's inequality to ensure security against coherent attacks for the finite-key analysis. Following established practices, we addressed the optimization procedures of Kato's inequality to further improve the final secure key rate. In simulations, our protocol achieves transmission distances exceeding 200 km with a misalignment error rate of 1.5%, and over 150 km even with a higher misalignment error rate of 4.5%, demonstrating its applicability in field tests.

Furthermore, we experimentally demonstrate our QSS protocol using nine sets of tests at a 30-dB channel loss, including a 5-km fiber distance. Varying the pulse intensities and X -basis selection probabilities, we achieve secure key rates ranging from 432 to 192 bps. In our implementation, the key factor influencing the final key rates is the X -basis selection probability. A high proportion of X basis results in a smaller number of detection events under the Y basis, implying increasing statistical fluctuation of Y basis and ultimately decreasing the secure key rate. When the dataset is sufficiently large to neglect statistical fluctuations, increasing the selection probability can further improve the secure key rate. Additionally, pulse intensity and QBERs in the X and Y bases also influence the key rate. Increasing the pulse intensity can enhance key rates, but at the risk of leaking more information and increasing the phase error rate. Therefore, choosing appropriate pulse intensities and X -basis selection probabilities is crucial for optimizing the final key rates.

Looking ahead, the development of multiuser QSS protocols is essential for realizing large-scale quantum net-

works and enabling more complex multiparty quantum communication tasks. Drawing inspiration from multiuser twin-field QKD implementations [68], we plan to investigate strategies for extending our QSS protocol to a greater number of users. This will involve exploring techniques like time-division multiplexing, advanced synchronization methods, and potentially alternative network architectures to address the challenges of scalability in QSS. Having achieved information-theoretic security and validation in real optical systems, our protocol offers a valuable reference for practical applications of multiparty quantum communication and the realization of quantum multiparty computing networks.

ACKNOWLEDGMENTS

This work is supported by the National Natural Science Foundation of China (Grant No. 12274223), the Fundamental Research Funds for the Central Universities and the Research Funds of Renmin University of China (Grant No. 24XNKJ14), and the Program for Innovative Talents and Entrepreneurs in Jiangsu (Grant No. JSS-CRC2021484).

Appendix A: FINITE-KEY ANALYSIS

In this work, we use Kato's inequality instead of the commonly used Azuma's inequality as concentration inequality to provide security against coherent attacks by calculating the upper bound of the observed phase error rate \overline{E}_p , taking statistical fluctuations into account [62, 63]. Kato's inequality, applied to a sum of correlated random variables and their expected value, provides a tighter bound compared to the widely used Azuma's inequality, leading to a higher secret key rate. Kato's inequality is presented in its general form as follows: let ξ_1, \dots, ξ_n be a sequence of random variables which satisfies $0 \leq \xi_i \leq 1, (i = 1, 2, \dots, n)$. We define Λ_k as the sum of these variables, i.e. $\Lambda_k = \sum_{i=1}^k \xi_i$. Let

\mathcal{F}_k denote the σ -algebra generated by $\{\xi_1, \dots, \xi_k\}$, which is called the natural filtration of this sequence. For any $k, a \in \mathbb{R}$ and any b such that $b \geq |a|$, according to Kato's inequality we have that

$$\Pr \left[\sum_{i=1}^k E(\xi_i | \mathcal{F}_{i-1}) - \Lambda_k \geq [b + a(\frac{2\Lambda_k}{k} - 1)]\sqrt{k} \right] \quad (\text{A1})$$

$$\leq \exp \left[\frac{-2(b^2 - a^2)}{\left(1 + \frac{4a}{3\sqrt{k}}\right)^2} \right], \quad (\text{A2})$$

in which $E(\cdot)$ denotes the expected value. If we replace ξ_i with $1 - \xi_i$ and a with $-a$, we have another form of Kato's inequality,

$$\Pr \left[\Lambda_k - \sum_{i=1}^k E(\xi_i | \mathcal{F}_{i-1}) \geq [b + a(\frac{2\Lambda_k}{k} - 1)]\sqrt{k} \right] \quad (\text{A3})$$

$$\leq \exp \left[\frac{-2(b^2 - a^2)}{\left(1 - \frac{4a}{3\sqrt{k}}\right)^2} \right]. \quad (\text{A4})$$

To estimate the upper bound of the observed phase error rate \bar{E}_p , we denote the detector click event in the i th round as a Bernoulli random variable ξ_i , where $i = 1, 2, \dots, k$. If the detector clicks in the i th round, $\xi_i = 1$, otherwise $\xi_i = 0$. In this way, $\Lambda_k = \sum_{i=1}^k \xi_i$ denotes the observed value of the total number of detector click events during k rounds. To get the tightest upper bound of the observed phase error rate \bar{E}_p , we need to choose the optimal values for a and b for Eq. (A1) to minimize the deviation $[b + a(\frac{2\Lambda_k}{k} - 1)]$. We define ϵ_a as the failure probability for estimating the upper bound, which satisfies $\epsilon_a = \exp \left[\frac{-2(b^2 - a^2)}{\left(1 + \frac{4a}{3\sqrt{k}}\right)^2} \right]$. The solution to the optimization problem can be found in [64, 65], which is

$$a_1 = a_1(\Lambda_k, k, \epsilon_a) \quad (\text{A5})$$

$$= \frac{3 \left(72\sqrt{k}\Lambda_k(k - \Lambda_k) \ln \epsilon_a - 16k^{3/2} \ln^2 \epsilon_a + 9\sqrt{2}(k - 2\Lambda_k)\sqrt{-k^2 \ln \epsilon_a(9\Lambda_k(k - \Lambda_k) - 2k \ln \epsilon_a)} \right)}{4(9k - 8 \ln \epsilon_a)(9\Lambda_k(k - \Lambda_k) - 2k \ln \epsilon_a)} \quad (\text{A6})$$

$$b_1 = b_1(a_1, k, \epsilon_a) = \frac{\sqrt{18a_1^2 k - (16a_1^2 + 24a_1\sqrt{k} + 9k) \ln \epsilon_a}}{3\sqrt{2k}} \quad (\text{A7})$$

By substituting a_1 and b_1 into Eq. (A1), we obtain the expression for the upper bound of the expected value,

$$\Lambda_k^* \leq \bar{\Lambda}_k^* = \Lambda_k + \Delta_1(a_1, b_1, k, \Lambda_k), \quad (\text{A8})$$

in which we use Λ_k^* to denote the expected value $\sum_{i=1}^k E(\xi_i | \mathcal{F}_{i-1})$ and $\Delta_1(a_1, b_1, k, \Lambda_k) = [b_1 + a_1(\frac{2\Lambda_k}{k} - 1)]\sqrt{k}$.

Similarly, solving the optimization problem corresponding to Eq. (A3) yields the lower bound of the expected value. The solutions are

$$a_2 = a_2(\Lambda_k, k, \epsilon_a) \quad (\text{A9})$$

$$= \frac{3 \left(72\sqrt{k}\Lambda_k(k - \Lambda_k) \ln \epsilon_a - 16k^{3/2} \ln^2 \epsilon_a - 9\sqrt{2}(k - 2\Lambda_k)\sqrt{-k^2 \ln \epsilon_a(9\Lambda_k(k - \Lambda_k) - 2k \ln \epsilon_a)} \right)}{4(9k - 8 \ln \epsilon_a)(9\Lambda_k(k - \Lambda_k) - 2k \ln \epsilon_a)} \quad (\text{A10})$$

$$b_2 = b_2(a_2, k, \epsilon_a) = \frac{\sqrt{18a_2^2 k - (16a_2^2 - 24a_2\sqrt{k} + 9k) \ln \epsilon_a}}{3\sqrt{2k}}. \quad (\text{A11})$$

Thus, we obtain the lower bound

$$\Lambda_k^* \geq \underline{\Lambda}_k^* = \Lambda_k - \Delta_2(a_2, b_2, k, \Lambda_k), \quad (\text{A12})$$

where $\Delta_2(a_2, b_2, k, \Lambda_k) = [b_2 + a_2(\frac{2\Lambda_k}{k} - 1)]\sqrt{k}$.

The above results are used to transform observed values into expected values. However, our protocol also requires the conversion of expected values back into observed values, a process also facilitated by Kato’s inequality. Unlike the previous results, the observed value Λ_k used for computing the optimal parameters a_i, b_i (where $i = 1, 2$) is not directly observed and thus remains unknown. Following the method in Ref [64, 65], we set $a = 0$ and the failure probability to ϵ_b in Eq. (A1) and Eq. (A3), obtaining the following inequalities:

$$\sum_{i=1}^k E(\xi_i | \mathcal{F}_{i-1}) \leq \Lambda_k + \Delta \quad (\text{A13})$$

$$\sum_{i=1}^k E(\xi_i | \mathcal{F}_{i-1}) \geq \Lambda_k - \Delta \quad (\text{A14})$$

where $\Delta = \sqrt{\frac{1}{2}k \ln \epsilon_b^{-1}}$.

We now briefly describe the process of calculating the upper bound of the phase error rate \bar{E}_p using the above inequalities. Without loss of generality, assuming Bob is the eavesdropper, Alice’s raw key bits are divided into two parts based on her basis selection. When Alice selects the X basis, the raw key bits are used to generate the secure key and estimate the bit error rate E_b^X . When Alice selects the Y basis, the raw key bits are used to calculate the upper bound of the phase error rate \bar{E}_p . In the experiment, we denote the number of total detection events and the number of bit errors measured in the Y basis as n_Y and m_Y , respectively, and the number of total detection events measured in the X basis as n_X . We then use the experimentally observed value m_Y to calculate the upper bound of m'_Y , which is the expected number of bit errors. Noting that this process transforms the observed value into the expected value to estimate the upper bound, thus, we use Eq. (A8) to obtain the tightest bound. We utilize $E_b^{Y'} = m'_Y/n_Y$ to calculate the upper bound of the expected bit error rate in the Y basis $E_b^{Y'}$. Subsequently, Eq. (5) is employed to compute the expected phase error rate in the X basis E'_p . Then, we can obtain the expected value of the number of phase errors m'_p in the X basis by $m'_p = E'_p n_X$. Next, we use m'_p to calculate its upper bound \bar{m}_p . Noting that this process transforms the expected value into the observed number of phase errors in the X basis, thus, we use Eq. (A13) to obtain the tightest bound. Then we can obtain the upper bound of the phase error rate in the X basis \bar{E}_p with the formula $\bar{E}_p = \bar{m}_p/n_X$.

Appendix B: DETAILED EXPERIMENTAL DATA

The precalibrated losses are shown in Table II, including Cir, BSs, PMs, and PCs. “PM-A (C)” stands for the PM used by Alice (Charlie), whose model number is iXblue MPX-LN-0.1. “PM-B” stands for the PM used

TABLE II. Efficiencies of the elements of the measurement station.

Optical devices	Insertion loss (dB)
Cir 2 \rightarrow 3	0.49
BS-1	0.72
BS-2	0.68
PM-A	2.89
PM-B	3.01
PM-C	2.23
PC ₁	0.33
PC ₂	0.45

by Bob, whose model number is EOSPACE PM-5S5-10-PFA-PFA-UV. Detailed experimental data under different input values of pulse intensities μ and X -basis selection probabilities p_x are depicted in Tables III(a) \sim III(c), where n denotes the number of clicks in the X basis and Y basis. “Detected ABC” denotes the number of detection events when Alice, Bob, and Charlie, respectively add phases “A”, “B”, and “C” on pulses. Note that, the insertion loss of the PC consists of the back-end attenuation of the PC to the SPD. PC₁ (SPD₁) is on the branch connecting to the Cir while PC₂ (SPD₂) is connected to the BS.

TABLE III(a). Detailed experimental data under different input values of μ while p_x is 0.9.

μ	9×10^{-4}		8×10^{-4}		7×10^{-4}	
n	1 095 111		951 473		843 121	
Detector	SPD ₁	SPD ₂	SPD ₁	SPD ₂	SPD ₁	SPD ₂
Detected 000	95 331	553	84 372	486	72 840	475
Detected 0 π 0	620	99 726	651	83 870	536	80 265
Detected π 00	910	105 578	771	90 217	737	80 262
Detected $\pi\pi$ 0	92 196	1023	82 188	903	70 631	960
Detected 00 π	976	98 805	884	83 851	850	75 293
Detected 0 $\pi\pi$	94 686	1332	83 523	1379	73 857	1138
Detected π 0 π	92 208	1070	82 221	990	68 962	880
Detected $\pi\pi\pi$	960	101 433	997	86 326	807	78 385
Detected $0\frac{\pi}{2}\frac{\pi}{2}$	3	872	6	737	3	682
Detected $0\frac{3\pi}{2}\frac{\pi}{2}$	1597	11	1461	11	1317	8
Detected $\pi\frac{\pi}{2}\frac{\pi}{2}$	1471	9	1340	6	1169	17
Detected $\pi\frac{3\pi}{2}\frac{\pi}{2}$	10	872	8	783	3	691
Detected $0\frac{\pi}{2}\frac{3\pi}{2}$	668	10	505	7	457	5
Detected $0\frac{3\pi}{2}\frac{3\pi}{2}$	13	815	22	753	10	669
Detected $\pi\frac{\pi}{2}\frac{3\pi}{2}$	15	1512	17	1266	18	1123
Detected $\pi\frac{3\pi}{2}\frac{3\pi}{2}$	617	8	568	12	427	4
Detected $\frac{\pi}{2}0\frac{\pi}{2}$	736	5	662	5	535	5
Detected $\frac{\pi}{2}\frac{\pi}{2}\frac{\pi}{2}$	7	1329	7	1116	10	1015
Detected $\frac{3\pi}{2}0\frac{\pi}{2}$	20	1638	17	1433	16	1179
Detected $\frac{3\pi}{2}\frac{\pi}{2}\frac{\pi}{2}$	929	19	863	16	686	5
Detected $\frac{\pi}{2}0\frac{3\pi}{2}$	19	1280	17	1173	17	1024
Detected $\frac{\pi}{2}\frac{\pi}{2}\pi$	1588	19	1333	24	1213	19
Detected $\frac{3\pi}{2}0\frac{3\pi}{2}$	842	8	779	12	573	11
Detected $\frac{3\pi}{2}\frac{\pi}{2}\frac{3\pi}{2}$	14	1100	17	913	10	848

TABLE III(b). Detailed experimental data under different input values of μ while p_x is 0.8.

μ	9×10^{-4}		8×10^{-4}		7×10^{-4}	
n	1 102 508		968 713		845 563	
Detector	SPD ₁	SPD ₂	SPD ₁	SPD ₂	SPD ₁	SPD ₂
Detected 000	64 617	378	57 170	360	49 161	288
Detected 0 π 0	432	70 000	307	61 633	285	51 932
Detected π 00	687	74 842	553	66 464	432	56 295
Detected $\pi\pi$ 0	66 196	734	57 695	776	50 077	497
Detected 00 π	882	73 278	722	64 648	707	57 275
Detected 0 $\pi\pi$	68 275	1105	59 926	723	53 385	868
Detected π 0 π	69 821	910	61 279	877	54 250	1039
Detected $\pi\pi\pi$	752	68 463	555	60 641	702	53 639
Detected 0 $\frac{\pi}{2}$ $\frac{\pi}{2}$	48	4877	26	4448	22	3789
Detected 0 $\frac{3\pi}{2}$ $\frac{\pi}{2}$	5666	36	4783	30	4239	40
Detected $\pi\frac{\pi}{2}$ $\frac{\pi}{2}$	5065	46	4594	37	3892	45
Detected $\pi\frac{3\pi}{2}$ $\frac{\pi}{2}$	31	3880	25	3345	31	3098
Detected 0 $\frac{\pi}{2}$ $\frac{3\pi}{2}$	3171	63	2861	42	2410	41
Detected 0 $\frac{3\pi}{2}$ $\frac{3\pi}{2}$	75	5032	59	4341	48	3839
Detected $\pi\frac{\pi}{2}$ $\frac{3\pi}{2}$	51	4113	48	3609	52	3293
Detected $\pi\frac{3\pi}{2}$ $\frac{3\pi}{2}$	3907	54	3349	49	3005	68
Detected $\frac{\pi}{2}$ 0 $\frac{\pi}{2}$	4690	41	4155	48	3583	33
Detected $\frac{\pi}{2}$ π $\frac{\pi}{2}$	24	3908	18	3459	20	2944
Detected $\frac{3\pi}{2}$ 0 $\frac{\pi}{2}$	40	4123	43	3597	41	3124
Detected $\frac{3\pi}{2}$ π $\frac{\pi}{2}$	4407	62	3816	63	3468	64
Detected $\frac{\pi}{2}$ 0 $\frac{3\pi}{2}$	58	5130	57	4680	89	3930
Detected $\frac{\pi}{2}$ π $\frac{3\pi}{2}$	4094	59	3599	55	3088	59
Detected $\frac{3\pi}{2}$ 0 $\frac{3\pi}{2}$	4998	107	4275	107	3787	125
Detected $\frac{3\pi}{2}$ π $\frac{3\pi}{2}$	75	4755	72	4031	71	3574

TABLE III(c). Detailed experimental data under different input values of μ while p_x is 0.7.

μ	9×10^{-4}		8×10^{-4}		7×10^{-4}	
n	1 102 207		968 120		856 672	
Detector	SPD ₁	SPD ₂	SPD ₁	SPD ₂	SPD ₁	SPD ₂
Detected 000	41 129	225	37 040	205	31 484	155
Detected 0 π 0	282	53 911	256	46 024	254	41 576
Detected π 00	530	47 769	429	41 448	291	36 086
Detected $\pi\pi$ 0	46 439	558	41 190	387	34 844	354
Detected 00 π	606	50 815	523	44 696	392	40 961
Detected 0 $\pi\pi$	41 134	613	36 582	469	32 605	367
Detected π 0 π	44 719	654	39 529	589	34 123	460
Detected $\pi\pi\pi$	562	47 248	417	40 998	408	37 666
Detected 0 $\frac{\pi}{2}$ $\frac{\pi}{2}$	69	8841	57	7781	63	6892
Detected 0 $\frac{3\pi}{2}$ $\frac{\pi}{2}$	7646	82	6837	53	6245	71
Detected $\pi\frac{\pi}{2}$ $\frac{\pi}{2}$	7863	93	7048	58	5937	62
Detected $\pi\frac{3\pi}{2}$ $\frac{\pi}{2}$	61	7834	54	6837	57	6373
Detected 0 $\frac{\pi}{2}$ $\frac{3\pi}{2}$	7859	170	7142	139	5893	131
Detected 0 $\frac{3\pi}{2}$ $\frac{3\pi}{2}$	166	9127	133	7971	107	7621
Detected $\pi\frac{\pi}{2}$ $\frac{3\pi}{2}$	141	8478	129	7384	118	6584
Detected $\pi\frac{3\pi}{2}$ $\frac{3\pi}{2}$	7433	120	6721	121	5737	121
Detected $\frac{\pi}{2}$ 0 $\frac{\pi}{2}$	8209	81	7441	65	6393	64
Detected $\frac{\pi}{2}$ π $\frac{\pi}{2}$	56	8369	46	6983	44	6445
Detected $\frac{3\pi}{2}$ 0 $\frac{\pi}{2}$	133	9706	110	8576	87	7587
Detected $\frac{3\pi}{2}$ π $\frac{\pi}{2}$	7972	107	6910	80	6076	82
Detected $\frac{\pi}{2}$ 0 $\frac{3\pi}{2}$	146	8894	141	7743	128	7086
Detected $\frac{\pi}{2}$ π $\frac{3\pi}{2}$	8826	184	7718	118	6835	139
Detected $\frac{3\pi}{2}$ 0 $\frac{3\pi}{2}$	7244	215	6496	182	5487	149
Detected $\frac{3\pi}{2}$ π $\frac{3\pi}{2}$	139	7097	105	6050	110	5722

-
- [1] H. J. Kimble, The quantum internet, *Nature* **453**, 1023 (2008).
- [2] N. Gisin and R. Thew, Quantum communication, *Nat. Photonics* **1**, 165 (2007).
- [3] S. Wehner, D. Elkouss, and R. Hanson, Quantum internet: A vision for the road ahead, *Science* **362**, eaam9288 (2018).
- [4] C. H. Bennett and G. Brassard, Quantum cryptography: Public key distribution and coin tossing, *Theor. Comput. Sci.* **560**, 7 (2014).
- [5] A. K. Ekert, Quantum cryptography based on bell's theorem, *Phys. Rev. Lett.* **67**, 661 (1991).
- [6] T. Sasaki, Y. Yamamoto, and M. Koashi, Practical quantum key distribution protocol without monitoring signal disturbance, *Nature* **509**, 475 (2014).
- [7] C.-X. Weng, R.-Q. Gao, Y. Bao, B.-H. Li, W.-B. Liu, Y.-M. Xie, Y.-S. Lu, H.-L. Yin, and Z.-B. Chen, Beating the fault-tolerance bound and security loopholes for byzantine agreement with a quantum solution, *Research* **6**, 0272 (2023).
- [8] M. Lucamarini, Z. L. Yuan, J. F. Dynes, and A. J. Shields, Overcoming the rate–distance limit of quantum key distribution without quantum repeaters, *Nature* **557**, 400 (2018).
- [9] H.-L. Yin, Y. Fu, C.-L. Li, C.-X. Weng, B.-H. Li, J. Gu, Y.-S. Lu, S. Huang, and Z.-B. Chen, Experimental quantum secure network with digital signatures and encryption, *Natl. Sci. Rev.* **10**, nwac228 (2023).
- [10] Y.-A. Chen, Q. Zhang, T.-Y. Chen, W.-Q. Cai, S.-K. Liao, J. Zhang, K. Chen, J. Yin, J.-G. Ren, Z. Chen, *et al.*, An integrated space-to-ground quantum communication network over 4,600 kilometres, *Nature* **589**, 214 (2021).
- [11] L. Zhou, J. Lin, Y.-M. Xie, Y.-S. Lu, Y. Jing, H.-L. Yin, and Z. Yuan, Experimental quantum communication overcomes the rate-loss limit without global phase tracking, *Phys. Rev. Lett.* **130**, 250801 (2023).
- [12] S. Wang, Z.-Q. Yin, D.-Y. He, W. Chen, R.-Q. Wang, P. Ye, Y. Zhou, G.-J. Fan-Yuan, F.-X. Wang, W. Chen, *et al.*, Twin-field quantum key distribution over 830-km fibre, *Nat. Photon.* **16**, 154 (2022).
- [13] J. Gu, X.-Y. Cao, Y. Fu, Z.-W. He, Z.-J. Yin, H.-L. Yin, and Z.-B. Chen, Experimental measurement-device-independent type quantum key distribution with flawed and correlated sources, *Sci. Bull.* **67**, 2167 (2022).
- [14] C.-L. Li, Y. Fu, W.-B. Liu, Y.-M. Xie, B.-H. Li, M.-G. Zhou, H.-L. Yin, and Z.-B. Chen, All-photonic quantum repeater for multipartite entanglement generation, *Opt. Lett.* **48**, 1244 (2023).
- [15] X.-Y. Cao, B.-H. Li, Y. Wang, Y. Fu, H.-L. Yin, and Z.-B. Chen, Experimental quantum e-commerce, *Sci. Adv.* **10**, eadk3258 (2024).
- [16] K. Azuma, K. Tamaki, and H.-K. Lo, All-photonic quantum repeaters, *Nat. Commun.* **6**, 6787 (2015).
- [17] B. Fröhlich, J. F. Dynes, M. Lucamarini, A. W. Sharpe, Z. Yuan, and A. J. Shields, A quantum access network, *Nature* **501**, 69 (2013).
- [18] X. Jing, C. Qian, C.-X. Weng, B.-H. Li, Z. Chen, C.-Q. Wang, J. Tang, X.-W. Gu, Y.-C. Kong, T.-S. Chen, *et al.*, Experimental quantum byzantine agreement on a three-user quantum network with integrated photonics, *Sci. Adv.* **10**, eadp2877 (2024).
- [19] P. Schiаны, J. Kalb, E. Sztatecsny, M.-C. Roehsner, T. Guggemos, A. Trenti, M. Bozzio, and P. Walther, Demonstration of quantum-digital payments, *Nat. Commun.* **14**, 3849 (2023).
- [20] C.-L. Li, Y. Fu, W.-B. Liu, Y.-M. Xie, B.-H. Li, M.-G. Zhou, H.-L. Yin, and Z.-B. Chen, Breaking the rate-distance limitation of measurement-device-independent quantum secret sharing, *Phys. Rev. Research* **5**, 033077 (2023).
- [21] M. De Oliveira, I. Nape, J. Pinnell, N. TabeBordbar, and A. Forbes, Experimental high-dimensional quantum secret sharing with spin-orbit-structured photons, *Phys. Rev. A* **101**, 042303 (2020).
- [22] B. P. Williams, J. M. Lukens, N. A. Peters, B. Qi, and W. P. Grice, Quantum secret sharing with polarization-entangled photon pairs, *Phys. Rev. A* **99**, 062311 (2019).
- [23] R. Cleve, D. Gottesman, and H.-K. Lo, How to share a quantum secret, *Phys. Rev. Lett.* **83**, 648 (1999).
- [24] M. Hillery, V. Bužek, and A. Berthiaume, Quantum secret sharing, *Phys. Rev. A* **59**, 1829 (1999).
- [25] Y. Fu, H.-L. Yin, T.-Y. Chen, and Z.-B. Chen, Long-distance measurement-device-independent multiparty quantum communication, *Phys. Rev. Lett.* **114**, 090501 (2015).
- [26] Y. Zhou, J. Yu, Z. Yan, X. Jia, J. Zhang, C. Xie, and K. Peng, Quantum secret sharing among four players using multipartite bound entanglement of an optical field, *Phys. Rev. Lett.* **121**, 150502 (2018).
- [27] H. Lu, Z. Zhang, L.-K. Chen, Z.-D. Li, C. Liu, L. Li, N.-L. Liu, X. Ma, Y.-A. Chen, and J.-W. Pan, Secret sharing of a quantum state, *Phys. Rev. Lett.* **117**, 030501 (2016).
- [28] B. Bell, D. Markham, D. Herrera-Martí, A. Marin, W. Wadsworth, J. Rarity, and M. Tame, Experimental demonstration of graph-state quantum secret sharing, *Nat. Commun.* **5**, 5480 (2014).
- [29] K.-J. Wei, H.-Q. Ma, and J.-H. Yang, Experimental circular quantum secret sharing over telecom fiber network, *Opt. Express* **21**, 16663 (2013).
- [30] A. Shamir, How to share a secret, *Commun. ACM* **22**, 612 (1979).
- [31] G. R. Blakley, Safeguarding cryptographic keys, in *Managing requirements knowledge, international workshop on* (IEEE Comput. Soc., 1979) pp. 313–313.
- [32] L. K. Grover, A fast quantum mechanical algorithm for database search, in *Proceedings of the twenty-eighth annual ACM symposium on Theory of computing* (ACM Press, 1996) pp. 212–219.
- [33] P. W. Shor, Polynomial-time algorithms for prime factorization and discrete logarithms on a quantum computer, *SIAM Rev.* **41**, 303 (1999).
- [34] G.-P. Guo and G.-C. Guo, Quantum secret sharing without entanglement, *Phys. Rev. A* **310**, 247 (2003).
- [35] Z. Gao, T. Li, and Z. Li, Deterministic measurement-device-independent quantum secret sharing, *Sci. China-Phys. Mech. Astron.* **63**, 120311 (2020).
- [36] F.-G. Deng, H.-Y. Zhou, and G. L. Long, Circular quantum secret sharing, *J. Phys. A: Math. Theor.* **39**, 14089 (2006).
- [37] D. Markham and B. C. Sanders, Graph states for quantum secret sharing, *Phys. Rev. A* **78**, 042309 (2008).

- [38] S.-J. Qin, F. Gao, Q.-Y. Wen, and F.-C. Zhu, Cryptanalysis of the hillery-bužek-berthiaume quantum secret-sharing protocol, *Phys. Rev. A* **76**, 062324 (2007).
- [39] F.-L. Yan and T. Gao, Quantum secret sharing between multiparty and multiparty without entanglement, *Phys. Rev. A* **72**, 012304 (2005).
- [40] F.-G. Deng, X.-H. Li, H.-Y. Zhou, and Z.-j. Zhang, Improving the security of multiparty quantum secret sharing against trojan horse attack, *Phys. Rev. A* **72**, 044302 (2005).
- [41] L. Xiao, G. L. Long, F.-G. Deng, and J.-W. Pan, Efficient multiparty quantum-secret-sharing schemes, *Phys. Rev. A* **69**, 052307 (2004).
- [42] A. M. Lance, T. Symul, W. P. Bowen, B. C. Sanders, and P. K. Lam, Tripartite quantum state sharing, *Phys. Rev. Lett.* **92**, 177903 (2004).
- [43] J. Bogdanski, N. Rafei, and M. Bourennane, Experimental quantum secret sharing using telecommunication fiber, *Phys. Rev. A* **78**, 062307 (2008).
- [44] S. Gaertner, C. Kurtsiefer, M. Bourennane, and H. Weinfurter, Experimental demonstration of four-party quantum secret sharing, *Phys. Rev. Lett.* **98**, 020503 (2007).
- [45] C. Schmid, P. Trojek, M. Bourennane, C. Kurtsiefer, M. Żukowski, and H. Weinfurter, Experimental single qubit quantum secret sharing, *Phys. Rev. Lett.* **95**, 230505 (2005).
- [46] Y.-A. Chen, A.-N. Zhang, Z. Zhao, X.-Q. Zhou, C.-Y. Lu, C.-Z. Peng, T. Yang, and J.-W. Pan, Experimental quantum secret sharing and third-man quantum cryptography, *Phys. Rev. Lett.* **95**, 200502 (2005).
- [47] A. Tavakoli, I. Herbauts, M. Żukowski, and M. Bourennane, Secret sharing with a single d-level quantum system, *Phys. Rev. A* **92**, 030302 (2015).
- [48] M. Hai-Qiang, W. Ke-Jin, and Y. Jian-Hui, Experimental single qubit quantum secret sharing in a fiber network configuration, *Opt. Lett.* **38**, 4494 (2013).
- [49] G. P. He, Comment on “experimental single qubit quantum secret sharing”, *Phys. Rev. Lett.* **98**, 028901 (2007).
- [50] C. Schmid, P. Trojek, M. Bourennane, C. Kurtsiefer, M. Żukowski, and H. Weinfurter, Schmid et al. reply, *Phys. Rev. Lett.* **98**, 028902 (2007).
- [51] F. Xu, X. Ma, Q. Zhang, H.-K. Lo, and J.-W. Pan, Secure quantum key distribution with realistic devices, *Rev. Mod. Phys.* **92**, 025002 (2020).
- [52] J. Gu, X.-Y. Cao, H.-L. Yin, and Z.-B. Chen, Differential phase shift quantum secret sharing using a twin field, *Opt. Express* **29**, 9165 (2021).
- [53] Z.-Y. Jia, J. Gu, B.-H. Li, H.-L. Yin, and Z.-B. Chen, Differential phase shift quantum secret sharing using a twin field with asymmetric source intensities, *Entropy* **23**, 716 (2021).
- [54] K. Inoue, T. Ohashi, T. Kukita, K. Watanabe, S. Hayashi, T. Honjo, and H. Takesue, Differential-phase-shift quantum secret sharing, *Opt. Express* **16**, 15469 (2008).
- [55] J. Gu, Y.-M. Xie, W.-B. Liu, Y. Fu, H.-L. Yin, and Z.-B. Chen, Secure quantum secret sharing without signal disturbance monitoring, *Opt. Express* **29**, 32244 (2021).
- [56] K. Wei, X. Yang, C. Zhu, and Z.-Q. Yin, Quantum secret sharing without monitoring signal disturbance, *Quantum Inf. Process.* **17**, 230 (2018).
- [57] A. Shen, X.-Y. Cao, Y. Wang, Y. Fu, J. Gu, W.-B. Liu, C.-X. Weng, H.-L. Yin, and Z.-B. Chen, Experimental quantum secret sharing based on phase encoding of coherent states, *Sci. China-Phys. Mech. Astron.* **66**, 260311 (2023).
- [58] H.-K. Lo and J. Preskill, Security of quantum key distribution using weak coherent states with nonrandom phases, *Quantum Inf. Comput.* **7**, 431 (2007).
- [59] M. Koashi, Simple security proof of quantum key distribution based on complementarity, *New J. Phys.* **11**, 045018 (2009).
- [60] M. Curty, K. Azuma, and H.-K. Lo, Simple security proof of twin-field type quantum key distribution protocol, *npj Quantum Inf.* **5**, 64 (2019).
- [61] H.-L. Yin and Z.-B. Chen, Finite-key analysis for twin-field quantum key distribution with composable security, *Sci. Rep.* **9**, 17113 (2019).
- [62] G. Kato, Concentration inequality using unconfirmed knowledge, arXiv:2002.04357 (2020).
- [63] K. Azuma, Weighted sums of certain dependent random variables, *Tohoku Math. J. (2)* **19**, 357 (1967).
- [64] G. Currás-Lorenzo, Á. Navarrete, K. Azuma, G. Kato, M. Curty, and M. Razavi, Tight finite-key security for twin-field quantum key distribution, *npj Quantum Inf.* **7**, 22 (2021).
- [65] M.-Y. Li, X.-Y. Cao, Y.-M. Xie, H.-L. Yin, and Z.-B. Chen, Finite-key analysis for coherent one-way quantum key distribution, *Phys. Rev. Research* **6**, 013022 (2024).
- [66] S. K. Joshi, D. Aktas, S. Wengerowsky, M. Lončarić, S. P. Neumann, B. Liu, T. Scheidl, G. C. Lorenzo, Ž. Samec, L. Kling, *et al.*, A trusted node-free eight-user metropolitan quantum communication network, *Sci. Adv.* **6**, eaba0959 (2020).
- [67] Y. Qin, J. Cheng, J. Ma, D. Zhao, Z. Yan, X. Jia, C. Xie, and K. Peng, Efficient and secure quantum secret sharing for eight users, *Phys. Rev. Research* **6**, 033036 (2024).
- [68] X. Zhong, W. Wang, R. Mandil, H.-K. Lo, and L. Qian, Simple multiuser twin-field quantum key distribution network, *Phys. Rev. Applied.* **17**, 014025 (2022).